UC Berkeley

Title

Graphene-polyelectrolyte multilayer membranes with tunable structure and internal charge

Permalink

Authors

Liu, Yang

Zheng, Sunxiang

Gu, Ping

et al.

Publication Date

DOI

Peer reviewed

Graphene-Polyelectrolyte Multilayer Membranes with Tunable Structure and Internal Charge

Revision Submitted to

Carbon

December 20, 2019

Yang Liu,[a, b] Sunxiang Zheng,[a,#] Ping Gu,[b] Andrew J. Ng,[a] Monong Wang,[a] Yangyang Wei[c], Jeffrey J. Urban[d] and Baoxia Mi[a*]

[a] Department of Civil and Environmental Engineering, University of California,
Berkeley, California 94720, United States

[b] School of Environmental Science and Engineering, Tianjin University, Tianjin 300072, China

[c] The Institute of Seawater Desalination and Multipurpose Utilization, State Oceanic Administration, Tianjin 300192, China

[d] The Molecular Foundry, Lawrence Berkeley National Laboratory, Berkeley, California 94720, United States

---

** Corresponding author. e-mail: mib@berkeley.edu; tel.: +1-510-664-7446.
# Co-first author

Abstract

One great advantage of graphene-polyelectrolyte multilayer (GPM) membranes is their tunable structure and internal charge for improved separation performance. In this study, we synthesized GO-dominant GPM membrane with internal negatively-charged domains, polyethyleneimine (PEI)-dominant GPM membrane with internal positively-charged domains and charged-balanced dense/loose GPM membranes by simply adjusting the ionic strength and pH of the GO and PEI solutions used in layer-by-layer membrane synthesis. A combined system of quartz crystal microbalance with dissipation (QCM-D) and ellipsometry was used to analyze the mass deposition, film thickness, and layer density of the GPM membranes. The performance of the GPM membranes were compared in terms of both permeability and selectivity to determine the optimal membrane structure and synthesis strategy. One effective strategy to improve the GPM membrane permeability-selectivity tradeoff is to assemble charged-balanced dense membranes under weak electrostatic interactions. This balanced membrane exhibits the highest $MgCl_2$ selectivity (~86%). Another effective strategy for improved cation removal is to create PEI-dominant membranes that provide internal positively-charged barrier to enhance cation selectivity without sacrificing water permeability. These findings shine lights on the development of a systematic approach to push the boundary of permeability-selectivity tradeoff for GPM membranes.

1. Introduction

Graphene oxide (GO), a two-dimensional (2D) carbon-based nanosheet, has been studied intensively as an interesting material for making water-purification membranes.[1-5] However, due to the well-known swelling issues (i.e., expansion of interlayer spacing or even resuspension) in the aqueous solutions,[6, 7] stabilization of the GO layers is a key step toward any real applications. Till now, many stabilization methods have been proposed, including physical confinement by polymer matrix,[3] chemical crosslinking, [8-10] cationic bonding,[11] and others. [12]

Among various synthesis methods, layer-by-layer (LbL) assembly has gained popularity as a facile, scalable, and cost-effective strategy.[13, 14] An LbL assembly process typically involves the successive adsorption of two materials via attractive forces such as electrostatic interaction, van der Waals (vdW) interaction, and hydrogen bonding.[15-18] For example, a positively charged polycation and a negatively charged polyanion can be sequentially adsorbed onto a substrate via electrostatic interactions without any chemical reaction.[19] Due to the presence of ionizable carboxylic groups, GO is negatively charged in neutral and basic solutions, and hence can be considered as a unique 2D polyanion. Therefore, GO layers can be stabilized through the LbL assembly of GO and a positively charged polycation to form GO-polyelectrolyte multilayer (GPM) membranes. Recent studies have demonstrated several promising environmental applications of GPM membranes, such as pervaporation and dehydration,[20] heavy metal removal,[21] divalent cation removal,[22] and organic dye removal.[23-25]

The ionic strength and pH of the membrane synthesis environment can alter the charge properties and structure of the GPM membranes, and hence affect their performance in removing ionic and organic species.[14] Therefore, it is potentially feasible to actively control membrane structure and charge properties by adjusting the ionic strength and pH of the synthesis solutions during the LbL assembly process. The alternating adsorption of polyelectrolytes in LbL assembly is mainly driven by electrostatic interactions and self-terminated when charge neutralization is reached.[26] The availability of charged sites on polyelectrolytes can be adjusted by solution pH, and the strength of electrostatic interaction force could be greatly affected by ionic strength of the solution. Attempts have been made to tune multilayer polyelectrolyte membranes by adding sodium chloride into one or both polyelectrolyte solutions.[27-29] It was found that the thickness of each polyelectrolyte layer can be changed by salt addition.[27] However, as a unique polyanion, GO has very different morphology and response to the aqueous environment compared to the conventional polymer-based polyelectrolytes, thus potentially resulting in very different multilayer membranes. However, the effects of synthesis conditions on the properties and performance of GPM membranes have rarely been discussed and the corresponding mechanisms are largely lacking.

To address the above issue, we thoroughly investigated the effects of ionic strength and pH on the properties of suspended GO and polyethyleneimine (PEI), which are used in the synthesis of GPM membranes using LbL assembly. A hydrolyzed polyacrylonitrile (hPAN) membrane with negatively-charged surface was selected as the substrate for the GPM membranes. A combined system of quartz crystal microbalance with dissipation (QCM-D) and ellipsometry was employed to precisely monitor the mass deposition and film thickness of GO and PEI in each deposition cycle. The structure and charge properties of the GPM membranes assembled under different ionic strength and pH conditions were analyzed and optimized. The membrane performance was evaluated in terms of water

permeability and selectivity tradeoff. Based on our findings, potential strategies to enhance the separation performance of GPM membranes were proposed.

2. Experimental

2.1. Chemicals and materials

Polyethyleneimine (PEI, Mw 750,000), polyacrylonitrile (PAN, Mw 150,000), N,N-dimethylformamide (DMF), and lithium chloride (LiCl) were used as received from Sigma-Aldrich (St. Louis, MO). Sodium chloride (NaCl), hydrogen chloride (HCl), and sodium hydroxide (NaOH) were used as received from Fisher Chemical (Fair Lawn, NJ). The hPAN membrane substrate was made by using a conventional phase-inversion method followed by partial hydrolyzation in 1.5 M NaOH solution for 1.5 h.[30] The pure water permeability and zeta potential of hPAN substrate were characterized as 22 LMH/bar and -67.0 mV, respectively. GO was prepared from graphite using the modified Hummers' method as described in our previous work.[8, 13]

2.2. LbL assembly of the GO-polyelectrolyte multilayer (GPM) membranes

As a positively charged polyelectrolyte with high charge density[16, 31], PEI was used in this study to neutralize the negatively charged GO nanosheets in the layer-by-layer (LbL) assembly of the GO-polyelectrolyte multilayer (GPM) membranes. The concentrations of both GO and PEI solutions was 1 g/L. The procedure for the LbL assembly of a GPM membrane is illustrated in Fig. 1. After hydrolysis, the negatively charged hPAN membrane substrate was soaked in PEI solution for 30 min, allowing the deposition of PEI, followed by thoroughly rinsing the substrate with deionized (DI) water to remove any loosely bounded PEI from the membrane surface. The membrane was then soaked in GO solution for another 30 min, followed by DI water rinsing. With such a cycle of alternating PEI and GO deposition, a double layer (DL) of GO-PEI was formed. The above deposition cycle was repeated several times to fabricate the GPM membrane with a desired number of double layers. To

investigate the ionic strength effect, NaCl was added into the GO and PEI solutions while maintaining a neutral pH. To study the pH effect, the ionic strength of GO and PEI solutions was controlled at 100 mM by NaCl addition, and the pH was adjusted using 0.1 M NaOH or HCl.

Fig.1. Schematic illustration of the LbL assembly of GPM membranes.

2.3. Membrane and Material Characterization

The zeta potential and hydrodynamic diameter of GO and PEI in solutions were measured by Zetasizer Nano ZS90 (Malvern Instruments, UK). The assembled GPM membranes were characterized using X-ray photoelectron (XPS) spectroscopy (PHI 5400, Perkin-Elmer, Eden Prairie, MN) to determine chemical functional groups and elemental composition. The surface charge and morphology of the GPM membranes were characterized using Zetasizer and atomic force microscope (AFM, Dimension Icon, Bruker, Santa Barbara, CA) respectively. An integrated system of quartz crystal microbalance with dissipation (QCM-D, E-1, Q-sense, Sweden) and ellipsometry (FS-1 Multi-wavelength, Film Sense, Lincoln, NE) was employed to monitor the consecutive assembly of GO and PEI layers on a gold sensor. Detailed information on sample preparation and data analysis can be found in the supplementary data.

2.4. Membrane performance tests

Membrane performance was evaluated using a lab-scale cross-flow nanofiltration (NF) system under a trans-membrane pressure of 50 psi (3.4 bar) at room temperature (20 °C). Water permeability was recorded using a digital balance (Denver Instruments, Denver, CO). Feed solutions contain one of the following representative ionic species: $MgCl_2$ (10 mM), $CaCl_2$ (10 mM), Na_2SO_4 (10 mM), and NaCl (30 mM) or one of Methylene blue (MB, 7.5 mg/L) and Rhodamine-WT (R-WT, 7.5 mg/L) as model organic species. The concentration of ionic species in the permeate was measured by a conductivity meter (Accumet Excel XL30, Thermo Scientific, Marietta, OH). The concentrations of MB and R-WT were determined using a UV-vis spectrophotometer (UV160U, Shimadzu Scientific Instruments, Columbia, MD) at wavelengths of 655 and 590 nm, respectively. The apparent rejection of the ionic and organic species was calculated using Eq. 1.

$$R = \left(1 - \frac{C_P}{C_F}\right) \times 100\%$$

(1)

where C_P and C_F stand for the concentrations of ionic/organic species in the permeate and in the feed, respectively.

3. Results and discussion

3.1. Effects of ionic strength and pH on GO and PEI properties

The freshly synthesized GO, as characterized by XPS in Fig. 2(a), is abundant with oxygenated function groups, which occupy a total of ~58% of the carbon atoms in the basal plane. In particular, the ionizable carboxylic groups cause the GO to be negatively charged with a zeta potential of -40 mV in neutral and basic solutions, as shown in Fig. 2(b). PEI is a branched

polyelectrolyte that is positively charged with a zeta potential of +40 mV in neutral and acidic solutions due to the repeating units containing amine groups. When NaCl is added to increase the ionic strength of GO and PEI solutions, the surface charge of GO and PEI are screened by the excessive counterions (i.e., Na^+ and Cl^-), leading to a decrease in the absolute value of zeta potential. As shown in Fig. 2(b), the zeta potential of GO and PEI becomes -25 mV and 30 mV, respectively, in 100 mM NaCl solutions. It is worth noticing that multivalent ions like Ca^{2+} and Mg^{2+} potentially form coordinative complex with GO [32, 33], causing their aggregation and precipitation in solutions, hence are not used to study the effects of ionic strength.
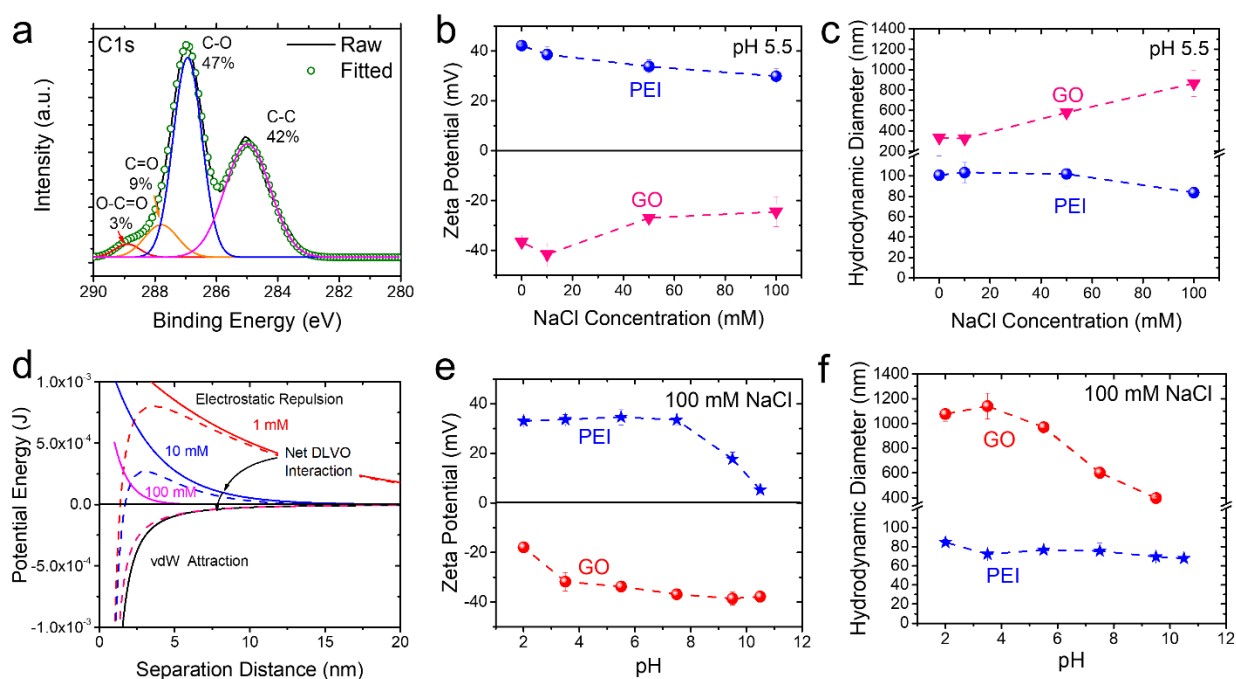
Fig. 2. Characterizations of the properties of GO and PEI in solutions. (a) The composition of carbon peaks in the XPS spectrum of GO to demonstrate the degree of oxidation. The effects of NaCl concentration on the zeta potential (b) and hydrodynamic diameters (c) of suspended GO and PEI in solutions. (d) Analysis of the energy potential between GO nanosheets as a function of separation distance based on DLVO theory. The effects of pH on the zeta potential (e) and hydrodynamic diameters (f) of suspended GO and PEI in solutions.

Interestingly, the ionic strength has opposite effects on the size of GO and PEI in solutions. As shown in Fig. 2(c), the hydrodynamic diameter of PEI decreases with increasing ionic strength, most likely because the repulsive electrostatic force between the charged amine groups on its polymeric chain becomes weaker at higher ionic strength, leading to a more coiled and denser chain structure. Whereas the hydrodynamic diameter of GO increases with increasing ionic strength. This is possibly because the less repulsive electrostatic forces between suspended GO nanosheets cause them to restack and aggregate, forming larger particles in the solution. To confirm this hypothesis, we calculated the vdW attractive force and electrostatic repulsion force between two aligned GO nanosheets (with detailed calculation discussed in the supplementary data). The attractive and repulsive forces and their sum, which gives the net DLVO interaction force, are plotted as a function of separation distance in Fig. 2(d). As the ionic strength increases from 1 to 100 mM, the vdW attraction remains constant, but the electrostatic repulsion decreases significantly. Consequently, the energy barrier/repulsive peak depicted by the net DLVO interaction curve becomes much weaker at higher ionic strength, suggesting the likelihood of forming GO aggregates in solutions.

Solution pH can also affect the charge and size of GO and PEI due to the protonation/deprotonation of charged functional groups, i.e., the carboxylic groups on GO and amine groups on PEI.[34-36] The carboxylic functional group on GO is a weak acid with a pKa of around 4 [37], similar to that of isolated carboxylic groups[38]. Therefore, as pH gradually increases from 2 to 11, the zeta potential of GO becomes more negative (Fig. 2(d)) due to the deprotonation of carboxylic groups (Fig. 2(e)). Correspondingly, the hydrodynamic diameter of GO increases from 300 to 1100 nm with decreasing pH (Fig. 2(f)) because of the formation of GO aggregates at low pH when the electrostatic repulsion between GO is weak. For PEI, the zeta potential measurements in Fig. 2(e) depict a pKa value of around 8.5 [39], lower than that of isolated amine groups (~10). This is because the amine

groups on the PEI polymeric chain are densely packed, resulting in steric effects on the deprotonation reaction[40]. Therefore, the zeta potential of PEI remains almost constant at ~35 mV in acidic and neutral environment (pH below 8), but sharply decreases to around 5 mV when pH increases above 9 due to the deprotonation of amine groups. As a result of the change in zeta potential, the weakly charged PEI chains become more coiled and looped, slightly reducing the hydrodynamic diameter of PEI (Fig.2 (f)).

3.2. Tailoring the structure of GPM membranes by adjusting ionic strength

Since ionic strength can affect the charge and size of GO and PEI in solution, it is possible to tailor the structure of GPM membranes by adjusting the ionic strength of GO and PEI solutions. In order to understand the GPM membrane structure, a combined QCM-D and ellipsometry analysis was used to online monitor the mass and thickness of the membrane at each step of the LbL deposition. As shown in Fig. 3(a) and 3(b), when 100 mM NaCl was added to increase the ionic strength of GO and PEI solutions during the LbL deposition, both deposited mass and membrane thickness increase more dramatically than that without salt addition. After depositing 4 double layers (DL) of PEI and GO, the mass of the GPM membrane with salt addition becomes around 4 times and thickness almost 6 times of that without salt. Note that the addition of salt also increases the amount of deposited GO much more dramatically than PEI. As shown in Fig. 3(a), the blue dashed line exhibits a much higher step increase for GO than PEI when NaCl is added, while the mass increase of GO and PEI is comparable without salt addition (red line). For example, adding salt increases the GO deposition amount from ~300 ng/cm^2 to almost ~3000 ng/cm^2 in each LbL cycle, while the mass of PEI deposited in each cycle only increases from ~350 ng/cm^2 to ~700 ng/cm^2. It indicates that increasing the ionic strength not only increases the total mass and thickness of the assembled membrane, but also changes the relative amount of GO and PEI within the membrane.
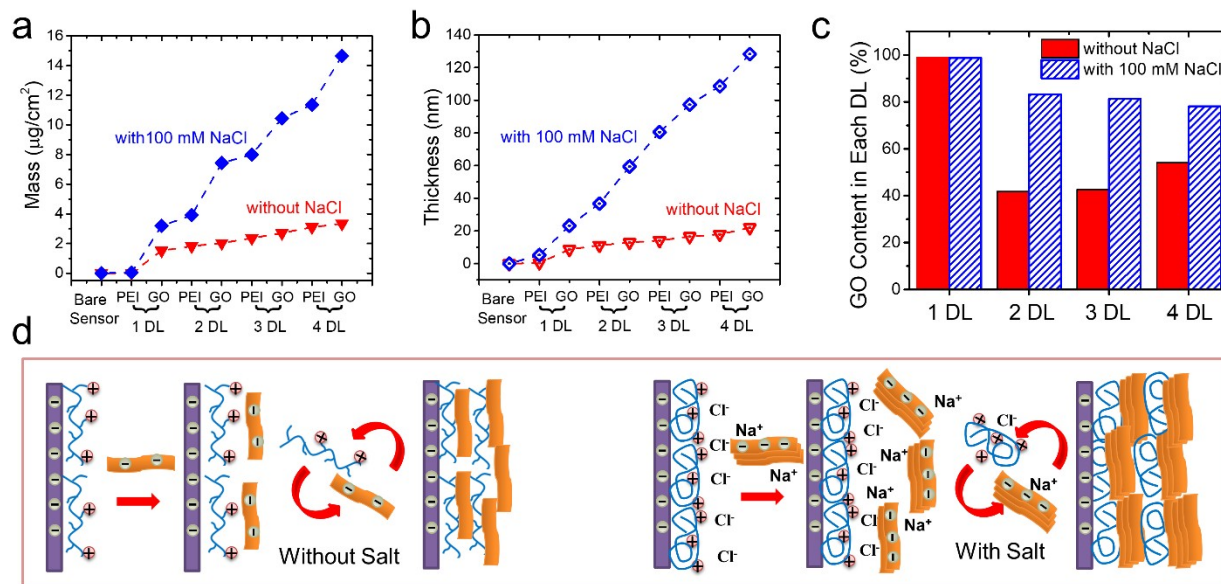
Fig. 3. Characterization of the mass (a) and thickness (b) of the GPM membranes during LbL assembly of GO and PEI with and without the addition of 100 mM NaCl. (c) Percentage of GO mass in each consecutive double layer (DL) of GO-PEI. (d) Schematic illustration of the LbL assembly of GO and PEI and the structure of thus synthesized GPM membrane with and without salt.

A more detailed composition analysis of the GPM membrane is shown in Fig. 3(c). GO is evidently the predominant material (~97%) in the first DL with or without NaCl addition. However, in the subsequently deposited DLs with NaCl addition, GO consistently accounts for ~80% of the total mass, while in the DL without NaCl addition, GO only contributes to less than 50% of the total mass. Such differences in the deposition behavior of GO and PEI can be attributed to their conformational change in solutions with/without salt. As schematically illustrated in Figure 3(d), the PEI polymer chains are more stretched at low ionic strength due to the repulsive force between the ionizable head groups and they tend to lay flat when deposited[15]. At higher ionic strength, although the hydrodynamic diameter of PEI decreases as the polymer chain coil up (Fig. 2(c)), the coiled structure leads to an increase in the layer thickness in deposition[41, 42]. Therefore, although the fine morphology of the deposited PEI may differ slightly, the total mass and thickness of the deposited PEI layer do not change dramatically at high or

low ionic strength. On the other hand, GO preassembles/grows into larger particles with less exposed surface charges at high ionic strength, their deposition thus results in a much thicker GO layer in the synthesized GPM membrane. Therefore, the LbL assembly at high ionic strength leads to a GO-dominant GPM membrane, while low ionic strength results in a GO-PEI balanced membrane composition.

3.3. Water Permeability and Selectivity of the GPM membranes tailored by adjusting ionic strength

The GPM membranes synthesized at different ionic strengths are expected to exhibit different performances due to the structural and compositional changes. In order to understand the effects, we evaluated the water flux and ion rejection of the GPM membranes with 2.5 DL of GO-PEI, which were tailored by changing ionic strength. The outermost layer of a 2.5-DL GPM membrane is PEI, thus the membrane surface is positively charged, enabling the rejection of divalent cations (e.g., Mg^{2+}, Ca^{2+}) by Donnan exclusion effect. As shown in Figure 4(a), the water permeability of GPM membranes decreases with increasing ionic strength, most likely due to the increasing membrane thickness, as demonstrated earlier. Note that the most dramatic change takes place between zero and 10 mM NaCl, the water permeability drops from 20 to 3.6 LMH/bar when only 10 mM NaCl was added and remains almost constant despite any further increase in ionic strength. The rejection of $MgCl_2$ by the GPM membrane increases with increasing NaCl concentration. It jumps from 10% without NaCl addition to ~50% with the addition of 10 mM NaCl. Unlike the trend in water permeability though, the $MgCl_2$ rejection keeps increasing when more salt is added until it reaches ~75% with the addition of 100 mM NaCl. Such an increase in rejection can again be attributed to the increased membrane thickness at higher ionic strength. It indicates that the hindered diffusion of ions within the GPM membrane must also play a very important role in the cation rejection in addition to Donnan charge exclusion effects.

When NaCl is added in the LbL assembly of GPM membranes, it only takes a small number of DLs to obtain the desired membrane performance. As shown in Fig. 4(b), the rejection of $MgCl_2$ already reaches ~70% upon the deposition of 1.5 DLs (i.e., PEI-GO-PEI), and slightly increases to ~80% after the deposition of 4.5 DLs. The water permeability almost remains constant at 3.5 LMH/bar when the deposition cycle increases from 1.5 to 4.5 DLs. It indicates that adding NaCl could become an effective strategy to minimize the number of deposition cycles needed in LbL membrane synthesis.
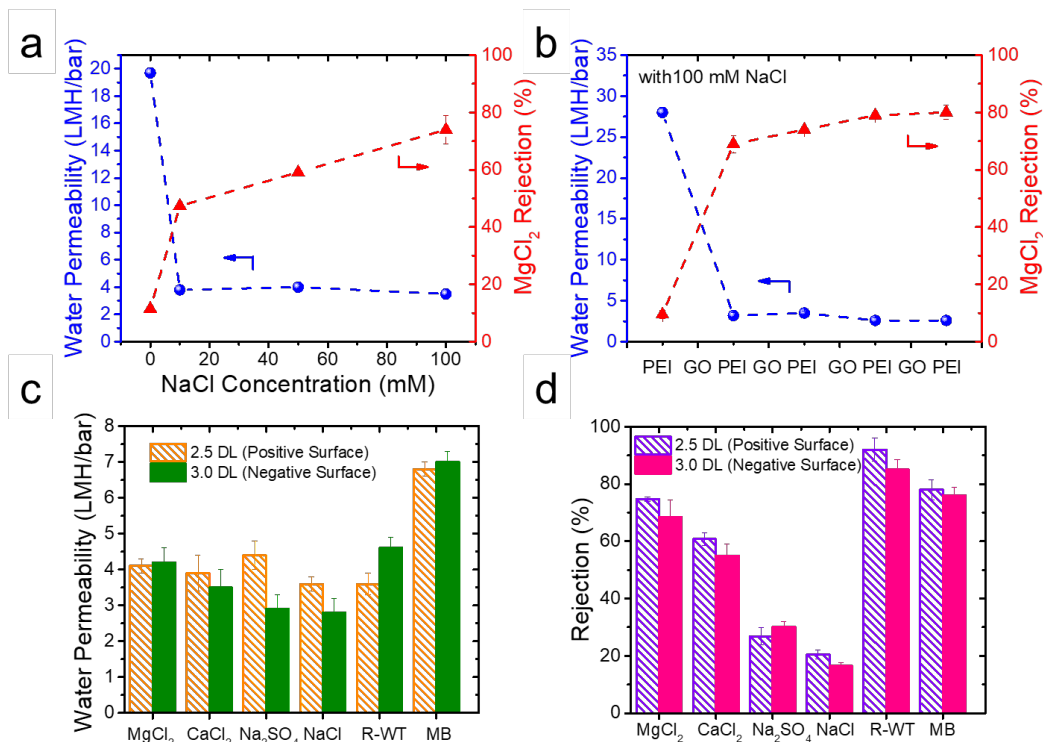
Fig. 4. Characterization of the GPM membrane performance. (a) The water permeability and 10 mM $MgCl_2$ rejection by a 2.5-DL GPM membrane assembled in solutions with different NaCl concentration. (b) Effects of deposited GO and PEI layers on the water permeability and 10 mM $MgCl_2$ rejection of GPM membranes. Effects of surface charge on the water permeability (c) and solute rejection (d) of a GPM membrane tested with feed water containing various solutes. To maintain a constant ionic strength, the concentration of $MgCl_2$, $CaCl_2$ and Na_2SO_4 solutions is 10 mM, and that of NaCl is 30 mM. The concentration of the organic dyes is 7.5 mg/L. The positive and negative surface charge was achieved by synthesizing a 2.5-DL membrane (with PEI as the outermost layer) and 3.0-DL membrane (with GO as the outermost layer), respectively. Both 2.5-DL and 3.0-DL membranes

were synthesized with the addition of 100 mM NaCl.

In order to understand the effects of membrane surface charge on the water permeability and cation rejection of GPM membranes, we compared the performance of a 2.5-DL membrane with positively charged PEI as the outermost layer and a 3-DL membrane with negatively charged GO as the outermost layer. The surface charge of the 2.5-DL membrane was measured to be 16 ± 3 mV and that of the 3.0 DL membrane was measured to be -28 ± 3 mV (Fig.S2). Fig. 4(c) shows that membrane surface charge does not affect water permeability of GPM membranes, as no significant difference was observed between the 2.5-DL and 3-DL membranes in the filtration experiments. The rejection of different solutes is compared in Fig. 4(d). The membrane surface charge only has minor effects on the rejection of different solutes. The membrane with positively charged surface has slightly higher rejection of divalent cations ($MgCl_2$ and $CaCl_2$) than negatively charged membrane, while the membrane with negatively charged surface has slightly higher rejection of divalent anions (Na_2SO_4) than positively charged membranes. Nevertheless, the overall effects of surface charge on solute rejection is very weak, indicating the rejection is dominated by internal properties of the GPM membranes instead of surface charge.

The internal charge of GPM membranes has a major effect on membrane selectivity, because as shown in Fig. 4(d), both positively and negatively charged GPM membranes have significantly higher rejection of $MgCl_2$ and $CaCl_2$ (> 60%) than that of Na_2SO_4 and NaCl (~ 20%). It is believed that within the GPM membrane structure there are predominant domains of PEI that offer dense internal positive charge and thus serve as an effective barrier to stop the passage of divalent cations (Mg^{2+}, Ca^{2+}) due to Donnan exclusion. There are predominant, negatively-charged domains of GO as well, but they cannot serve as effective barriers for divalent anions, most likely because the GO domains suffer severe swelling that results in large interlayer spacing to prevent it from serving as an effective barrier for SO_4^{2-}.

Therefore, although SO_4^{2-} ions are bigger than Mg^{2+} or Ca^{2+}, the rejection of SO_4^{2-} ions by GPM membranes are lower. When the solutes get bigger, however, size exclusion becomes the dominant separation mechanism and the effect of internal charge diminishes. For example, the GPM membrane has relatively high rejection of R-WT and MB regardless of their charge (R-WT being negatively charged, and MB being positively charged).

A unique benefit of tailoring the structure of GPM membranes using ionic strength during the LbL assembly process is that dominant GO and PEI domains that are either negatively or positively charged can be generated internally within the GPM membrane. Such internal negative/positive layers may serve as a charged barrier, thus leading to enhanced rejection of targeted cations or anions. For traditional NF membranes, the rejection of ions often relies on the surface charge of the membrane. A positively charged membrane surface is typically more effective in removing divalent cations due to Donnan charge exclusion. However, a positively charged membrane surface is more prone to fouling than negatively charged membranes because most natural organic matters and particles in water are negatively charged. Therefore, a positively charged membrane surface is usually avoided to prevent membrane fouling in water purification. To solve such a dilemma on surface charge, generating internal positively charged domains (i.e. PEI layers) to effectively remove divalent cations offer a novel approach to enhance the selectivity of membranes without scarifying their antifouling properties.

3.4. Synthesis and characterization of GO-dominant, PEI-dominant, and charge-balanced GPM membranes

The internal positively/negatively-charged domains within a GPM membrane can be further tailored by adjusting the pH of the GO and PEI solutions during the LbL assembly. Because the carboxylic groups on GO and amine groups on PEI have different pKa, varying pH can independently change the charge and deposition amount of GO and PEI. For example, a GO-dominant membrane

can be synthesized at pH 3.5. Because the carboxylic groups on GO (with a pKa of around 4) are protonated and carry less negative charge at pH 3.5, while the amine groups on PEI (with a pKa between 8 and 9) carry strong positive charge at pH 3.5, the charge neutralization between GO and PEI will result in more deposition of GO and form thick GO-dominant layers. QCM-D was used to monitor the formation of such domains during the LbL membrane assembly. As shown in Fig. 5(a), the cumulative deposition of GO and PEI at pH 3.5 demonstrates that the GO deposition results in a more dramatic mass increase than PEI. Overall, GO accounts for more than 80% of the total mass, confirming a GO-dominant membrane structure (Fig. 5(b)). Fig. 5(c) shows that thickness of the GO-dominant membrane is almost three times of the baseline GPM membrane (synthesized at neutral pH). The presence of GO domains can be visually observed in Fig. 5(d) as dark aggregated brownish spots on the surface. The AFM image in Fig. 5(e) also shows much rougher surface for the GO-dominant membrane, confirming the presence of aggregated GO domains. The density of the GO-dominant membrane is only around 1 g/cm^3, slightly lower than that of the baseline GPM membrane.   Our previous study showed that the density of layer-stacked GO membranes is high (~1.8 g/cm^3) when dry, but drops to ~ 1 g/cm^3 in aqueous solutions due to severe swelling.[6] Therefore, the low density of GO-dominant membranes indicates significant swelling of the GO domains, similar to that of layer-stacked GO membranes.

Under similar mechanisms, a PEI-dominant membrane can be synthesized at pH 9.5. The amine groups on PEI are partially deprotonated and lose some positive charge at pH 9.5, while the carboxylic groups on GO maintain strong negative charge. Therefore, the LbL assembly at pH 9.5 will increase the amount of PEI deposition and form PEI-dominant domains. However, because GO in general has lower charge-to-mass ratio than PEI, the absolute mass of PEI within the membrane is still slightly lower than GO. As shown in Fig. 5(b), PEI accounts for 41% of the total mass in the PEI-

dominant membrane, much higher than the 20% of PEI in a GO-dominant membrane. Fig. 5(c) demonstrates that the PEI-dominant membrane is both thicker (50 nm) and denser (1.6 g/cm^3) than the baseline GPM membrane (25 nm and 1.2 g/cm^3).
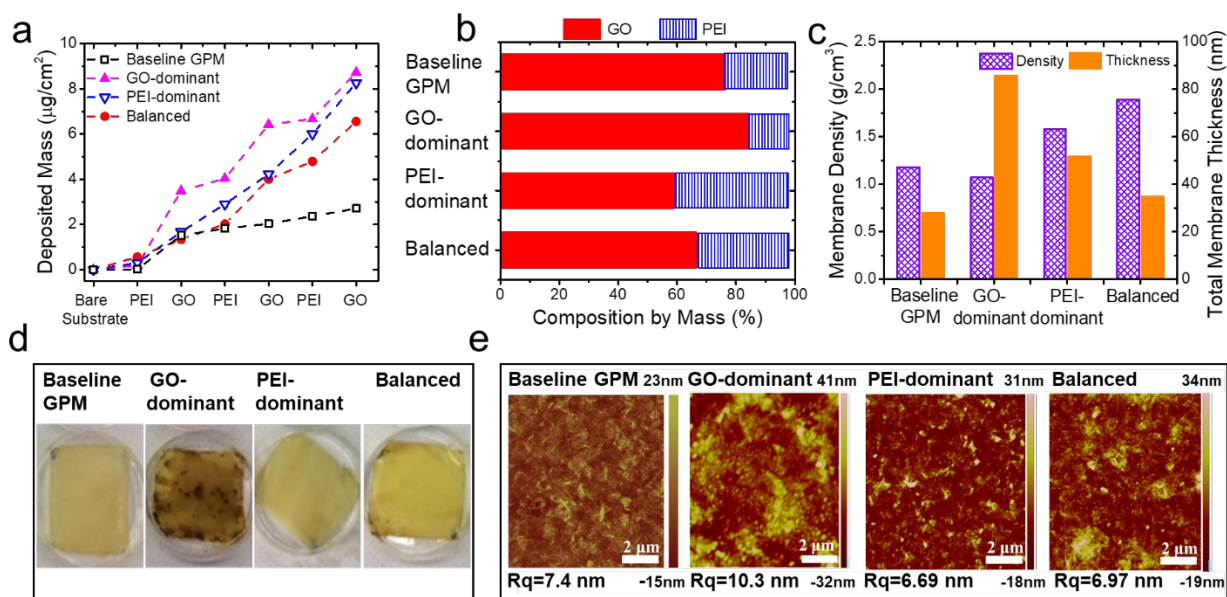

Fig. 5. Characterization of GO-dominant, PEI-dominant, and charge-balanced GPM membranes synthesized by adjusting pH of GO and PEI solutions. (a) Mass of GO and PEI layers deposited at different pH: GO dominant membranes synthesized at pH of 3.5 for both GO and PEI solutions, PEI-dominant membranes synthesized at pH of 9.5 for both GO and PEI solutions, balanced membranes synthesized at pH of 3.5 for GO and pH of 9.5 for PEI solutions, and baseline GPM membranes synthesized at neutral pH for both GO and PEI solutions. The composition (b), membrane density and thickness (c), visual observation (d), and AFM images (e) of GO-dominant, PEI-dominant, balanced and unadjusted membranes. All the membranes contain 3 DLs of GO and PEI.

It is also possible to purposely prepare a denser GPM membrane by independently adjusting the pH of GO and PEI solutions. As shown in Fig. 5(a), when the GO and PEI solutions have different pH (pH 3.5 for GO and pH 9.5 for PEI), both GO and PEI carry weaker charges and thus deposited less mass onto the membrane in each LbL deposition cycle. Such controlled deposition with weaker electrostatic interactions results in a more charge-balanced membrane with denser structures. Fig. 5(b) shows that the

balanced membrane contains 67% of GO in mass, which is smaller than the GO-dominant, but higher than the PEI-dominant membranes. The balanced membrane has the tightest structure among all GPM membranes. As demonstrated in Fig. 5(c), the balanced membrane has a density of ~1.8 g/cm^3, which is much higher than the GO-dominant (~1.0 g/cm^3) or PEI-dominant (~1.6 g/cm^3) membranes. In addition, the density of the balanced membrane in wet conditions is comparable to that of a layer-stacked GO membrane when it is dry.[6] In contrast to the swelling of GO-dominant membrane, the balanced membrane maintains a high layer density in aqueous solutions, suggesting that the balanced membrane has a well aligned layer structure that does not swell. This is most likely because the PEI plays a very important role in effectively stabilizing the GO layers and prevent them from swelling.

3.5. Optimization of the GPM membranes for improved divalent cation removal

In order to determine the optimized structure of GPM membranes for the best removal of divalent cations (e.g., MgCl$_2$), the performance of five different GPM membranes with 3 DLs of GO-PEI are summarized in Fig. 6. As being discussed earlier, tailoring the internal charged domains could result in membranes dominated with either GO or PEI. Fig. 6 shows that the GO-dominant membranes behave very similarly to the baseline-GPM membrane, which is synthesized at neutral pH. This is consistent with our earlier understanding that baseline-GPM membranes also have predominantly GO domains (Fig. 5(b)), although its GO content is slightly lower than GO-dominant membranes. Both baseline and GO-dominant membranes demonstrate poor removal of divalent cations, which can be attributed to the severe swelling of GO domains as discussed earlier.

An effective strategy to improve the rejection of divalent cations is to make denser structures. As shown in Fig. 6(a), the balanced membrane synthesized under weak electrostatic interactions provides the highest MgCl$_2$

rejection of 86%, although the membrane is relatively thin (~ 30 nm). The high rejection can be attributed to the dense and non-swelling structures of the balanced membrane. In addition, the PEI could potentially seal the defects and shortcuts between GO layers, which are believed to play a very important role in the low ion rejection by layer-stacked GO membranes.[43]

In order to understand the importance of membrane density, we also synthesized a charge-balanced but loose membrane using highly charged GO and PEI by adjusting the pH of GO and PEI solutions to 9.5 and 3.5, respectively. The strong electrostatic repulsion between individual PEI or GO molecules prevents them from being deposited closely to each other, causing loose structure with large voids in the synthesized membrane. Consequently, the loose membrane (marked as the star in Fig. 6) the highest water permeability (7.3 LMH/bar) but lowest $MgCl_2$ rejection (40%). The performance of the charge-balanced dense and loose membranes may represent two extreme conditions of the tradeoff relationship between the selectivity and permeability of GPM membranes. However, they represent an improved upper boundary (red dashed line in Fig. 6(a)) compared to the baseline and GO-dominant membranes (black dashed line) in the permeability-selectivity tradeoff analysis.

Fig. 6(a) reveals that the performance of the PEI-dominant membranes falls on the same permeability-selectivity tradeoff boundary as the charge-balanced GPM membranes. It suggests that PEI-dominant membranes have better performance than GO-dominant or baseline GPM membranes. Therefore, another potential strategy to improve divalent cation removal is to synthesize internal positively-charged domains that can serve as a charge barrier.
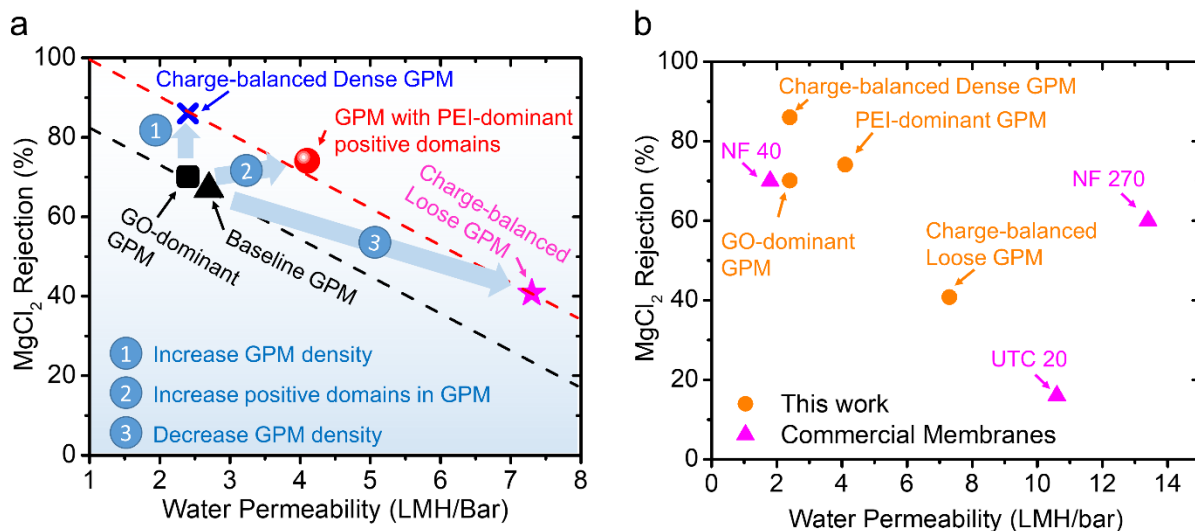
Fig. 6. (a) The permeability-selectivity tradeoff of GPM membranes with different structures and internal charge distributions. All the membranes contain 3 DLs of GO and PEI. There are three strategies to push the boundary of permeability-selectivity tradeoff of GPM membranes, including Route 1 of increasing the GPM density by creating charge-balanced deposition of thin and dense layers of graphene and polyelectrolyte; Route 2 of increasing positively-charged PEI domains inside the membrane while decreasing the overall mass deposition; and Route 3 of decreasing the GPM density by creating loose structures during deposition. (b) Comparison of the performances of GPM membranes and selected commercial membranes. [44-46]

Comparing the membrane performance associated with different membrane structures provides us some hints on developing membrane synthesis strategies to push the upper boundary of permeability-selectivity tradeoff. The most effective strategy seems to be making charge-balanced, thin, and dense membranes, going in the direction of route 1 in Fig. 6(a). Another feasible strategy is to increase positively-charged domains inside the membrane while decreasing the overall mass deposition/membrane thickness to simultaneously improve water permeability and selectivity, going in the direction of route 2 in Fig.6(a). As shown in Fig. 6(b), the charge balanced dense GPM membrane and the PEI-dominant membrane have demonstrated better selectivity than commercial NF membranes, such as NF

40 and NF 270 from Dow Chemical, the water permeability of the GPM membranes are higher than NF 40 but lower than NF 270. [44-46]

Decreasing membrane density will increase the number of large voids in the membrane structure thus increasing membrane permeability but usually accompanied by reduced selectivity (shown as route 3 in Fig. 6(a)). Therefore, to increase the water permeability while maintaining membrane selectivity, large voids need to be avoided. Instead, creating nanoscale pores on GO can provide additional transport path for water while preventing the passage of ions or molecules. Despite the challenges involved in drilling holes on GO, the availability of a large family of 2D materials (i.e., zeolite and MoS_2) could be potentially used to overcome some of the technical problems. [47-49] For example, Ye et al. reported the defect-engineered MoS_2 using oxygen plasma,[50] and 2D zeolite has recently been synthesized with 0.6 nm in-plane pores.[51] Since both of the materials are 2D nanosheets with negative charge, they can be used to substitute GO in the membrane fabrication. Therefore, this can potentially offer a path to further push the upper boundary of the permeability-selectivity tradeoff.

4. Conclusion

We have demonstrated that the structure and performance of GPM membranes can be optimized conveniently by adjusting the synthesis conditions, i.e. the ionic strength and pH of GO and PEI solutions. We synthesized GO-dominant, PEI-dominant, and charge-balanced dense and loose membranes and compared their performances in terms of permeability and selectivity tradeoff. Two effective strategies are identified to improve the GPM membrane permeability-selectivity tradeoff. One is to assemble charge-balanced dense and thin GPM membranes under weak electrostatic interactions by using high ionic strength and varying pH. This balanced membrane exhibits the highest $MgCl_2$ selectivity (~86%). Another strategy is to create PEI-dominant membranes that provide internal positively-charged

barrier to enhance cation selectivity without sacrificing water permeability. We also found that GO-dominant and loose membranes have poor selectivity either due to the swelling of GO domains or the existence of large voids that allow the passage of small ions. These findings shine lights on the development of a systematic approach to push the boundary of permeability-selectivity tradeoff for GPM membranes.

Acknowledgement

Reference

[1] F. Perreault, A. Fonseca de Faria, M. Elimelech, Environmental applications of graphene-based nanomaterials, Chem Soc Rev 44(16) (2015) 5861-96.

[2] H.Y. Yu, Y. Kang, Y.L. Liu, B. Mi, Grafting polyzwitterions onto polyamide by click chemistry and nucleophilic substitution on nitrogen: A novel approach to enhance membrane fouling resistance, Journal of Membrane Science 449 (2014) 50-57.

[3] J. Abraham, K.S. Vasu, C.D. Williams, K. Gopinadhan, Y. Su, C.T. Cherian, J. Dix, E. Prestat, S.J. Haigh, I.V. Grigorieva, P. Carbone, A.K. Geim, R.R. Nair, Tunable sieving of ions using graphene oxide membranes, Nat Nanotechnol (2017).

[4] H.M. Hegab, L. Zou, Graphene oxide-assisted membranes: Fabrication and potential applications in desalination and water purification, Journal of Membrane Science 484 (2015) 95-106.

[5] R.K. Joshi, P. Carbone, F.C. Wang, V.G. Kravets, Y. Su, I.V. Grigorieva, H.A. Wu, A.K. Geim, R.R. Nair, Precise and Ultrafast Molecular Sieving Through Graphene Oxide Membranes, Science 343(6172) (2014) 752-754.

[6] S. Zheng, Q. Tu, J.J. Urban, S. Li, B. Mi, Swelling of graphene oxide membranes in aqueous solution: characterization of interlayer spacing and insight into water transport mechanisms, ACS nano 11(6) (2017) 6440-6450.

[7] L. Jin, Z. Wang, S. Zheng, B. Mi, Polyamide-crosslinked graphene oxide membrane for forward osmosis, Journal of Membrane Science 545 (2018) 11-18.

[8] Y. Liu, E. Rosenfield, M. Hu, B. Mi, Direct observation of bacterial

deposition on and detachment from nanocomposite membranes embedded with silver nanoparticles, Water Research 47(9) (2013) 2949-2958.

[9] R.L.G. Lecaros, G.E.J. Mendoza, W.-S. Hung, Q.-F. An, A.R. Caparanga, H.-A. Tsai, C.-C. Hu, K.-R. Lee, J.-Y. Lai, Tunable interlayer spacing of composite graphene oxide-framework membrane for acetic acid dehydration, Carbon 123 (2017) 660-667.

[10] W.-S. Hung, Y.-H. Chiao, A. Sengupta, Y.-W. Lin, S.R. Wickramasinghe, C.-C. Hu, H.-A. Tsai, K.-R. Lee, J.-Y. Lai, Tuning the interlayer spacing of forward osmosis membranes based on ultrathin graphene oxide to achieve desired performance, Carbon 142 (2019) 337-345.

[11] L. Chen, G. Shi, J. Shen, B. Peng, B. Zhang, Y. Wang, F. Bian, J. Wang, D. Li, Z. Qian, G. Xu, G. Liu, J. Zeng, L. Zhang, Y. Yang, G. Zhou, M. Wu, W. Jin, J. Li, H. Fang, Ion sieving in graphene oxide membranes via cationic control of interlayer spacing, Nature (2017).

[12] A. Ghaffar, L. Zhang, X. Zhu, B. Chen, Scalable graphene oxide membranes with tunable water channels and stability for ion rejection, Environmental Science: Nano 6(3) (2019) 904-915.

[13] M. Hu, B. Mi, Layer-by-layer assembly of graphene oxide membranes via electrostatic interaction, Journal of Membrane Science 469 (2014) 80-87.

[14] Y. Oh, D.L. Armstrong, C. Finnerty, S. Zheng, M. Hu, A. Torrents, B. Mi, Understanding the pH-responsive behavior of graphene oxide membrane in removing ions and organic micropollulants, Journal of Membrane Science 541 (2017) 235-243.

[15] E. Kharlampieva, V. Kozlovskaya, S.A. Sukhishvili, Layer-by-Layer Hydrogen-Bonded Polymer Films: From Fundamentals to Applications, Advanced Materials 21(30) (2009) 3053-3065.

[16] T. Lee, S.H. Min, M. Gu, Y.K. Jung, W. Lee, J.U. Lee, D.G. Seong, B.-S. Kim, Layer-by-Layer Assembly for Graphene-Based Multilayer Nanocomposites: Synthesis and Applications, Chemistry of Materials 27(11) (2015) 3785-3796.

[17] M. Yang, Y. Hou, N.A. Kotov, Graphene-based multilayers: Critical evaluation of materials assembly techniques, Nano Today 7(5) (2012) 430-447.

[18] Y.H. Yang, L. Bolling, M.A. Priolo, J.C. Grunlan, Super gas barrier and selectivity of graphene oxide-polymer multilayer thin films, Adv Mater 25(4) (2013) 503-8.

[19] H. Tang, S. Ji, L. Gong, H. Guo, G. Zhang, Tubular ceramic-based multilayer separation membranes using spray layer-by-layer assembly, Polymer Chemistry 4(23) (2013) 5621.

[20] J. Zhao, Y. Zhu, F. Pan, G. He, C. Fang, K. Cao, R. Xing, Z. Jiang, Fabricating graphene oxide-based ultrathin hybrid membrane for pervaporation dehydration via layer-by-layer self-assembly driven by multiple interactions, Journal of Membrane Science 487 (2015) 162-172.

[21] Y. Zhang, S. Zhang, J. Gao, T.-S. Chung, Layer-by-layer construction of graphene oxide (GO) framework composite membranes for highly efficient heavy metal removal, Journal of Membrane Science 515 (2016) 230-237.

[22] Z.-B. Zhang, J.-J. Wu, Y. Su, J. Zhou, Y. Gao, H.-Y. Yu, J.-S. Gu, Layer-by-

layer assembly of graphene oxide on polypropylene macroporous membranes via click chemistry to improve antibacterial and antifouling performance, Applied Surface Science 332 (2015) 300-307.

[23] C. Liu, L. Shi, R. Wang, Crosslinked layer-by-layer polyelectrolyte nanofiltration hollow fiber membrane for low-pressure water softening with the presence of SO42− in feed water, Journal of Membrane Science 486 (2015) 169-176.

[24] Y. Lv, H.-C. Yang, H.-Q. Liang, L.-S. Wan, Z.-K. Xu, Nanofiltration membranes via co-deposition of polydopamine/polyethylenimine followed by cross-linking, Journal of Membrane Science 476 (2015) 50-58.

[25] Q. Nan, P. Li, B. Cao, Fabrication of positively charged nanofiltration membrane via the layer-by-layer assembly of graphene oxide and polyethylenimine for desalination, Applied Surface Science 387 (2016) 521-528.

[26] G. Rydzek, Q. Ji, M. Li, P. Schaaf, J.P. Hill, F. Boulmedais, K. Ariga, Electrochemical nanoarchitectonics and layer-by-layer assembly: from basics to future, Nano Today 10(2) (2015) 138-167.

[27] S.L. Clark, M.F. Montague, P.T. Hammond, Ionic effects of sodium chloride on the templated deposition of polyelectrolytes using layer-by-layer ionic assembly, Macromolecules 30(23) (1997) 7237-7244.

[28] J.E. Wong, A.M. Díez-Pascual, W. Richtering, Layer-by-Layer assembly of polyelectrolyte multilayers on thermoresponsive P (NiPAM-co-MAA) microgel: Effect of ionic strength and molecular weight, Macromolecules 42(4) (2008) 1229-1238.

[29] S.A. Sukhishvili, Responsive polymer films and capsules via layer-by-layer assembly, Current opinion in colloid & interface science 10(1-2) (2005) 37-44.

[30] Y. Kang, S. Zheng, C. Finnerty, M.J. Lee, B. Mi, Regenerable Polyelectrolyte Membrane for Ultimate Fouling Control in Forward Osmosis, Environ Sci Technol 51(6) (2017) 3242-3249.

[31] Q.T. Nguyen, K. Glinel, M. Pontié, Z. Ping, Immobilization of bio-macromolecules onto membranes via an adsorbed nanolayer, Journal of Membrane Science 232(1-2) (2004) 123-132.

[32] K.-S.L. Sungjin Park, Gulay Bozoklu, Weiwei Cai, SonBinh T. Nguyen, Rodney S. Ruoff, Graphene Oxide Papers Modified by Divalent Ions— Enhancing Mechanical Properties via Chemical Cross-Linking, ACS Nano 2(3) (2008) 572-578.

[33] C.N. Yeh, K. Raidongia, J. Shao, Q.H. Yang, J. Huang, On the origin of the stability of graphene oxide membranes in water, Nat Chem 7(2) (2014) 166-70.

[34] P.A. Nithya Joseph, Richard Hoogenboom, a.I.F.J. Vankelecom, Layer-by-layer preparation of polyelectrolyte multialyer membranes for separation, Polym. Chem. 5 (2014) 1817.

[35] J. Park, J. Park, S.H. Kim, J. Cho, J. Bang, Desalination membranes from pH-controlled and thermally-crosslinked layer-by-layer assembled multilayers, Journal of Materials Chemistry 20(11) (2010) 2085.

[36] S.Z. M. Elzb˙ieciak, P. Nowak,R. Krastev,M. Nowakowska,P. Warszyn´sk, Influence of pH on the Structure of Multilayer Films Composed of Strong and Weak Polyelectrolytes, Langmuir 25 (2009) 3255-3259.

[37] B. Konkena, S. Vasudevan, Understanding aqueous dispersibility of graphene oxide and reduced graphene oxide through p K a measurements, The journal of physical chemistry letters 3(7) (2012) 867-872.

[38] D.D. Perrin, B. Dempsey, E.P. Serjeant, pKa prediction for organic acids and bases, Springer1981.

[39] M. Mady, W. Mohammed, N.M. El-Guendy, A. Elsayed, Effect of polymer molecular weight on the DNA/PEI polyplexes properties, Rom J Biophys 21(2) (2011) 151-165.

[40] E. Shepherd, J. Kitchener, 474. The ionization of ethyleneimine and polyethyleneimine, Journal of the Chemical Society (Resumed) (1956) 2448-2452.

[41] L.K.a.B. Tieke, Selective Ion Transport across Self-Assembled Alternating Multilayers of Cationic and Anionic
Polyelectrolytes, Langmuir 16, (2000) 287-290.

[42] V.K. R, Internal structure of polyelectrolyte multilayer assemblies, Phys Chem Chem Phys 8(43) (2006) 5012-33.

[43] C.L. Ritt, J.R. Werber, A. Deshmukh, M. Elimelech, Monte Carlo Simulations of Framework Defects in Layered Two-Dimensional Nanomaterial Desalination Membranes: Implications for Permeability and Selectivity, Environmental Science & Technology 53(11) (2019) 6214-6224.

[44] L. Meihong, Y. Sanchuan, Z. Yong, G.J.J.o.M.S. Congjie, Study on the thin-film composite nanofiltration membrane for the removal of sulfate from concentrated salt aqueous: Preparation and performance, 310(1-2) (2008) 289-295.

[45] J. Schaep, B. Van der Bruggen, C. Vandecasteele, D.J.S. Wilms, P. Technology, Influence of ion size and charge in nanofiltration, 14(1-3) (1998) 155-162.

[46] M. Nyström, L. Kaipia, S.J.J.o.M.S. Luque, Fouling and retention of nanofiltration membranes, 98(3) (1995) 249-262.

[47] B. Mi, Scaling up nanoporous graphene membranes, Science 364(6445) (2019) 1033-1034.

[48] Z. Wang, Q. Tu, S. Zheng, J.J. Urban, S. Li, B. Mi, Understanding the Aqueous Stability and Filtration Capability of MoS2 Membranes, Nano Letters 17(12) (2017) 7289-7298.

[49] Y. Yang, X. Yang, L. Liang, Y. Gao, H. Cheng, X. Li, M. Zou, R. Ma, Q. Yuan, X. Duan, Large-area graphene-nanomesh/carbon-nanotube hybrid membranes for ionic and molecular nanofiltration, Science 364(6445) (2019) 1057-1062.

[50] G. Ye, Y. Gong, J. Lin, B. Li, Y. He, S.T. Pantelides, W. Zhou, R. Vajtai, P.M.J.N.l. Ajayan, Defects engineered monolayer MoS2 for improved hydrogen evolution reaction, 16(2) (2016) 1097-1103.

[51] M.Y. Jeon, D. Kim, P. Kumar, P.S. Lee, N. Rangnekar, P. Bai, M. Shete, B. Elyassi, H.S. Lee, K.J.N. Narasimharao, Ultra-selective high-flux membranes

from directly synthesized zeolite nanosheets, 543(7647) (2017) 690.